Control of electrostatic interactions between F-actin and genetically modified lysozyme in aqueous media

Lori K. Sanders*, Wujing Xian*, Camilo Guáqueta*, Michael J. Strohman*, Chuck R. Vrasich*, Erik Luijten*†‡§, and Gerard C. L. Wong*†‡§¶

Departments of *Materials Science and Engineering, †Physics, and ¶Bioengineering, ‡The Beckman Institute for Advanced Science and Technology, University of Illinois at Urbana–Champaign, Urbana, IL 61801-2920

Edited by Michael J. Welsh, University of Iowa College of Medicine, Iowa City, IA, and approved August 21, 2007 (received for review June 26, 2007)

The aim for deterministic control of the interactions between macroions in aqueous media has motivated widespread experimental and theoretical work. Although it has been well established that like-charged macromolecules can aggregate under the influence of oppositely charged condensing agents, the specific conditions for the stability of such aggregates can only be determined empirically. We examine these conditions, which involve an interplay of electrostatic and osmotic effects, by using a well defined model system composed of F-actin, an anionic rod-like polyelectrolyte, and lysozyme, a cationic globular protein with a charge that can be genetically modified. The structure and stability of actin–lysozyme complexes for different lysozyme charge mutants and salt concentrations are examined by using synchrotron x-ray scattering and molecular dynamics simulations. We provide evidence that supports a structural transition from columnar arrangements of F-actin held together by arrays of lysozyme at the threefold interstitial sites of the actin sublattice to marginally stable complexes in which lysozyme resides at twofold bridging sites between actin. The reduced stability arises from strongly reduced partitioning of salt between the complex and the surrounding solution. Changes in the stability of actin–lysozyme complexes are of biomedical interest because their formation has been reported to contribute to the persistence of airway infections in cystic fibrosis by sequestering antimicrobials such as lysozyme. We present x-ray microscopy results that argue for the existence of actin–lysozyme complexes in cystic fibrosis sputum and demonstrate that, for a wide range of salt conditions, charge-reduced lysozyme is not sequestered in ordered complexes while retaining its bacterial killing activity.

antimicrobial | cystic fibrosis | self-assembly | small-angle x-ray scattering | x-ray microscopy

In the presence of multivalent cations, strongly charged anionic polyelectrolytes such as DNA and F-actin can assemble into densely packed aggregates (1). The existence of this counterintuitive "like-charge attraction," which cannot be explained within the framework of mean-field approaches such as the Poisson–Boltzmann theory (2, 3), has motivated widespread experimental and theoretical work (4–6). In the case of F-actin bundles induced by multivalent ions, it has been shown that the ions within the bundles are correlated and hierarchically organized into density waves at polymer-length scales (7) but remain liquid-like at molecular-length scales (8). The problem becomes more complex when the mediating multivalent cations are replaced by spatially extended macroions, such as globular proteins. A macroion is characterized by a surface charge distribution and has its own counterions, as well as a significant excluded volume. In addition, in the presence of salt there is a strong interplay between electrostatic and osmotic effects. For example, in previous work, we have found that actin–lysozyme complexes are stable up to considerably higher salt concentrations than would be expected, because of osmotic pressure from ion partitioning that is constitutive of electrostatic binding between oppositely charged objects (9, 10).

The stability of these oppositely charged polyelectrolyte–protein complexes has important biomedical consequences. Accumulation of viscous mucus in pulmonary airways is the primary cause of long-term bacterial infections and eventually death in cystic fibrosis (CF) (11). Anionic polyelectrolytes such as F-actin (12) and DNA (13, 14) are released into the airway surface liquid when neutrophils and other cells lyse during the inflammatory response. The concentration of F-actin in the airway is reported to be 0.1–5 mg/ml and comprises ≈10% of total leukocyte protein (12). Together with anionic mucins, these polyelectrolytes cause the electrostatic assembly of large aggregates stabilized by cationic ligands, which commonly is observed in CF sputum (15–17). It has been suggested that endogenous antibacterial proteins, which are mostly cationic (e.g., lysozyme, lactoferrin, β-defensin, LL-37), constitute at least a portion of the ligands holding these anionic polyelectrolytes together (18). The concentration of the antibacterial lysozyme is estimated at 1 mg/ml in the CF airway (19). Because of their sequestration in polyelectrolyte complexes, the availability of antimicrobial proteins such as lysozyme is diminished significantly, and antimicrobial function in the airway is impaired correspondingly (20, 21). A biophysical understanding of antimicrobial polyelectrolyte binding thus can contribute to the rational design of therapeutic strategies.

In this article, we use genetically engineered lysozyme (22) with different monodisperse net charges (+9e, +5e, +3e) to understand and manipulate the stability of self-assembled actin–lysozyme complexes. Results from high-resolution synchrotron small-angle x-ray scattering (SAXS) and molecular dynamics (MD) simulations indicate that, as the lysozyme charge is reduced, actin–lysozyme complexes evolve from a high-stability phase (+9e lysozyme) to a low-stability phase (+5e and +3e lysozyme): The evidence suggests that the system evolves from complexes composed of hexagonally coordinated columnar arrangements of F-actin rods held together by 1D arrays of wild-type (WT) lysozyme at the threefold interstitial sites of the actin sublattice to complexes in which the 1D arrays of charge-reduced lysozyme are arranged at bridging sites between pairs of actin rods. Synchrotron x-ray microscopy using Fresnel zone-plate optics suggests that the high-stability phase of actin–lysozyme complexes may occur in sputum collected from CF patients, consistent with the expected behavior of strongly sequestered endogenous lysozyme with +9e charge. Interest-

Author contributions: L.K.S., W.X., E.L., and G.C.L.W. designed research; L.K.S., W.X., C.G., M.J.S., and C.R.V. performed research; L.K.S., C.G., E.L., and G.C.L.W. analyzed data; and L.K.S., E.L., and G.C.L.W. wrote the paper.

The authors declare no conflict of interest.

This article is a PNAS Direct Submission.

Abbreviations: CF, cystic fibrosis; SAXS, small-angle x-ray scattering; MD, molecular dynamics.

§To whom correspondence may be addressed at: Department of Materials Science and Engineering, University of Illinois at Urbana–Champaign, 1304 W. Green Street, Urbana, IL 61801-2920. E-mail: gclwong@uiuc.edu or luijten@uiuc.edu.

ingly, the low-stability phase containing charge-reduced lysozyme dissociates at a broad range of salt conditions, including the range reported for the airway, so that they are not sequestered by actin in close-packed complexes. This finding is independently confirmed by spectroscopic measurements of the free lysozyme concentration in actin–lysozyme mixtures with lysozyme of different charge. Moreover, bacterial killing assays show that the charge-reduced lysozyme mutants can retain most of the antimicrobial activity compared with the WT lysozyme against the PAO1 strain of *Pseudomonas aeruginosa*, a common opportunistic pathogen in CF, which suggests that it is possible to simultaneously minimize adventitious binding and retain activity in charge-optimized antimicrobials.

Results and Discussion

WT Lysozyme and F-Actin Self-Assemble into Stable Complexes at Physiological Conditions. First, we examine the complexation behavior of F-actin with WT bacteriophage T4 lysozyme. F-actin is an anionic rod-like cytoskeletal polymer (linear charge density $-e/0.25$ nm, persistence length 10 μm). WT T4 lysozyme (dimensions $30 \times 30 \times 50$ Å^3) is a cationic globular protein with a net charge of $+9e$ at physiological pH. In previous work (9, 10), we have demonstrated that F-actin forms ordered aggregates in the presence of hen egg-white lysozyme, which has a 3D structure different from WT T4 lysozyme (23). We confirm that WT T4 lysozyme also organizes F-actin into bundles. Fig. 1*a* shows a representative 2D SAXS diffraction pattern for partially aligned isoelectric lysozyme–actin bundles probed with a 300×300 μm^2 synchrotron x-ray beam, with associated 1D integrated intensity slices along the q_z and q_r directions shown in Fig. 1*b*. An inspection of the equatorial slice (q_r) shows a correlation peak at $q = 0.071$ Å^{-1} that corresponds to inter-actin packing in the composite actin–lysozyme bundles. Assuming the generic case of hexagonal coordination, this peak corresponds to an inter-actin spacing of ≈102 Å (Fig. 1*c*). The inter-actin space afforded by this structure corresponds well to the size required by interstitial lysozyme aligned with its long axis parallel to the actin rods. Other arrangements of lysozyme with different orientations and at different high-symmetry sites cannot generate peaks at this q position. In addition to this diffraction feature and weak mosaic-smeared intensity from the actin form factor (≈0.113 Å^{-1}), a new correlation peak at ≈0.128 Å^{-1} is observed along the meridional (q_z) direction, which corresponds to a correlation distance of ≈49.1 Å, roughly the length of T4 lysozyme along its long axis and consistent with the orientation and position of lysozyme inferred from the equatorial peak, indicating that lysozyme is close-packed along the actin filaments. These findings are in good accord with those for complexes of actin and hen egg-white lysozyme (9, 10), supporting the generic nature of actin–lysozyme complexation.

These x-ray observations are confirmed by a combination of grand-canonical Monte Carlo simulations and MD simulations of F-actin bundles to which a neutralizing amount of lysozyme has been added (10). Such complexes are found to have a vanishing net osmotic pressure (indicating stability) at an inter-actin spacing of 100 Å, in good agreement with the SAXS results. Moreover, the simulations reveal the spatial distribution of lysozyme within this complex (Fig. 1*d*). Under conditions of thermodynamic equilibrium, the proteins are concentrated in the threefold interstitial sites between the filaments, in full agreement with the structure inferred from the SAXS data (Fig. 1*c*). The numerical calculations also explicitly confirm that an even more expanded lattice structure, in which WT lysozyme is situated between pairs of actin filaments, is thermodynamically unfavorable and will contract. In addition, the simulations reproduce the close-packed arrangement of lysozyme with its long axis parallel to the actin axis.

Experimentally, we find that this actin–lysozyme structure also is stable in the presence of mucins, such as purified human MUC5B fragments, at physiological concentrations and that MUC5B does not form complexes with lysozyme (Fig. 1*e*). The

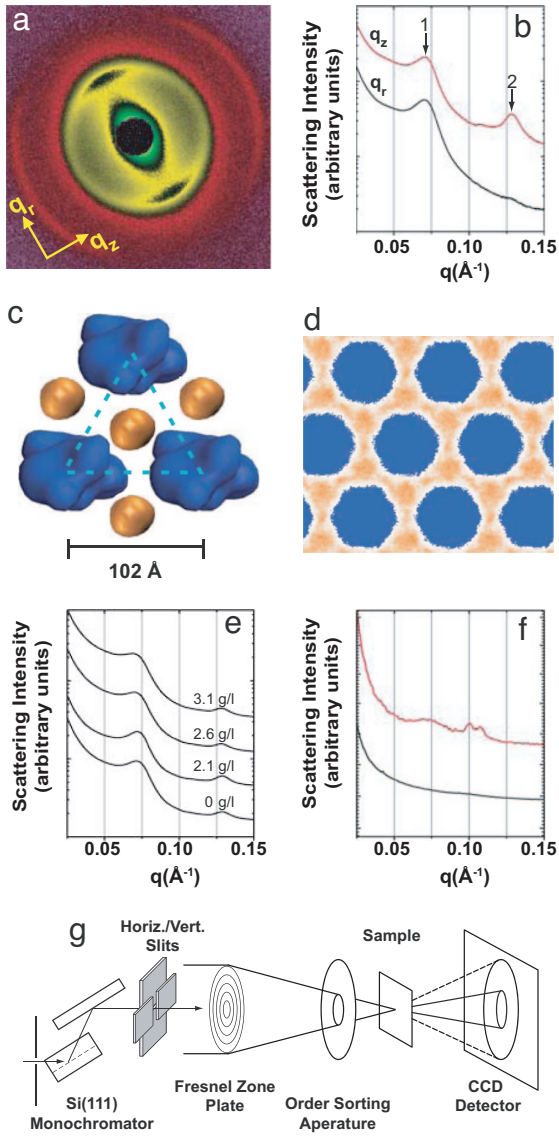

Fig. 1. Synchrotron x-ray measurements and MD simulations demonstrate that F-actin and WT lysozyme form stable, ordered complexes. (*a*) Synchrotron 2D x-ray diffraction pattern of partially aligned actin–WT lysozyme bundles self-assembled in a solution containing 100 mM NaCl. (*b*) 1D integrated slices along q_z (red line) and q_r (black line) directions with arrows marking the actin–actin close-packed bundling peak (*1*) and the lysozyme–lysozyme correlation peak (*2*). (*c*) Proposed model of actin–WT lysozyme bundle (end view) with WT lysozyme (orange) packed between actin filaments (blue). The x-ray data (*b*) indicate an inter-actin spacing of 102 Å, providing sufficient space for the presence of interstitial lysozyme. (*d*) Density plots from MD simulations showing the lysozyme distribution in the actin–WT lysozyme complexes without added salt. The lysozyme is located predominantly in the threefold interstitial regions. (*e*) Integrated diffraction data show that actin–lysozyme complexes are not significantly affected by the presence of human MUC5B fragments [at concentrations of 0 mg/ml (control) up to 3.1 mg/ml]. (*f*) 1D integration from x-ray microdiffraction measurements of CF sputum (red line), which shows a diffraction peak at $q \approx 0.07$ Å, consistent with actin–lysozyme complexes, along with peaks corresponding to self-assembly from other mucus components. The local character of the aggregates is demonstrated by the black curve, which is sampled at ≈200 μm from the sample shown in red but displays no signs of ordered structure. (*g*) Schematic diagram of the microdiffraction experiment at the Advanced Photon Source, Argonne, IL.

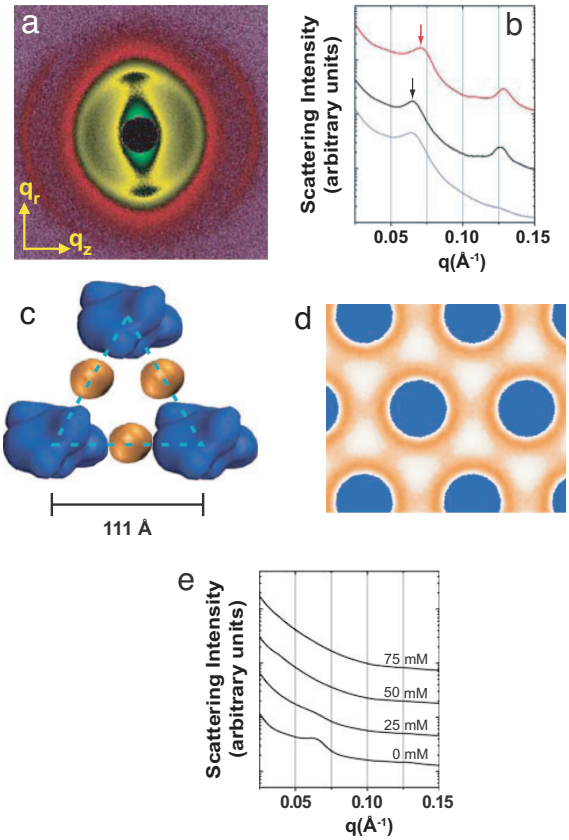

Fig. 2. Charge-reduced lysozyme forms complexes with F-actin that are structurally distinct from and less stable than those observed for WT lysozyme. (*a*) Synchrotron 2D x-ray diffraction pattern of partially aligned actin–mutant lysozyme bundles. (*b* and *c*) 1D integrated slices of actin–WT q_z (red line), actin–mutant q_z (black line), and actin–mutant q_r (gray line) directions. A shift in the position of the actin–actin bundling peak to lower *q*, as indicated by the arrows (*b*), suggests a change in lysozyme coordination in the complex from threefold sites (Fig. 1*c*) to twofold sites (*c*), thus shifting the inter-actin spacing from ≈102 Å to ≈111 Å. (*d*) Density plots showing the MD-simulated lysozyme distribution in the actin–lysozyme complexes without added salt. In contrast to the WT–lysozyme distribution (Fig. 1*d*), in the mutant lysozyme–actin complexes (*d*) the lysozyme is found strongly concentrated around the actin filaments with enhanced concentration in the twofold bridging sites with the threefold sites being nearly devoid of lysozyme. (*e*) 1D integrated slices of actin–triple-mutant lysozyme (+3e) in the q_r direction showing the actin–actin close-packed bundling peak at $q \approx 0.063$ Å^{-1}, which corresponds to an inter-actin spacing of ≈114 Å. This phase dissociates upon the addition of 25 mM NaCl.

addition of up to 3 mg/ml of MUC5B mucin fragments has no significant effect on the diffraction signature of actin–lysozyme bundles. A more stringent test of whether such complexes can exist in CF airway conditions, however, is a direct examination of sputum samples from CF patients. To investigate ordered structures within sputum, we employ x-ray microscopy techniques (Fig. 1 *f* and *g*) in which a 0.5×0.5 μm^2 beam is rastered across sputum samples, and the resultant spatially resolved diffraction data are collected. In addition to F-actin and lysozyme, CF sputum also consists of water, salts, DNA, various species of mucins, and other polymeric components and cell debris (24). Surprisingly, ordered structures indeed can be observed in CF sputum, despite its complex and heterogeneous nature. We clearly observe the presence of a correlation peak at $q \approx 0.07$ Å^{-1}, which is close to the characteristic diffraction peak from actin–lysozyme complexes (Fig. 1*f*, red line). Diffraction features near $q \approx 0.110$ Å^{-1} may be attributable to the helix form factor of moderately twist-distorted actin (25, 26) or may indicate possible additional self-assembly from other mucus components. The diffraction features are highly spatially localized: Examination of a representative grid of microdiffraction data shows that ordered aggregates have typical sizes of ≈100–200 μm and are embedded in a disordered matrix that only exhibits low-*q* scattering from density fluctuations but otherwise does not show discernable diffraction peaks (Fig. 1*f*, black line). This evidence argues for the existence of ordered actin–lysozyme complexes in disordered and heterogeneous CF mucus, the occurrence of which is unexpected. Because good surface charge-matching between antimicrobials and F-actin enhances the stability of bound complexes in salt solutions through the maximization of counterion release, a potential way to dissolve such complexes is to destroy the charge-matching by modifying the charge on lysozyme.

MD Simulations Predict That Charge-Reduced Lysozyme Forms a Low-Stability Phase with Lysozyme at Twofold "Bridging" Sites. To examine this hypothesis, we first employ MD simulations of a coarse-grained mixture of F-actin and lysozyme (10), where the net lysozyme charge is reduced from +9e (the value of WT lysozyme at physiological pH) to +5e. To maintain a charge-neutral mixture, the number of lysozyme molecules in the simulation cell is increased by a factor 9/5. We find that, in the absence of external salt, the charge-reduced lysozyme still is able to bundle the F-actin. However, instead of the threefold coordination observed for the WT lysozyme (Fig. 1*d*), we now find a strikingly different arrangement in which each lysozyme has a twofold coordination and forms a bridge between pairs of actin rods (Fig. 2*d*). This shift in geometry is accompanied by a shift in the inter-actin separation, resulting in a swelling of the bundle. The swelling significantly reduces the partitioning of any added monovalent salt and thus greatly diminishes the stabilizing effect observed for WT lysozyme (9), as is confirmed in Fig. 3 (gray line), where the complex is found to be unstable upon addition of even small amounts of monovalent salt. Indeed, already in a salt-free environment (Fig. 3, black line), the net osmotic pressure only barely reaches zero upon variation of the actin spacing and displays a very shallow negative region, indicating a low stability of the actin–lysozyme complex. It is instructive to compare the ionic distributions within complexes that are held together by WT and charge-reduced lysozyme, respectively (Fig. 4). Although the cross-sectional distribution of anions is rather homogeneous and similar in both cases (Fig. 4 *a* and *b*), the cation distributions are different. In the compact bundles containing WT lysozyme, the cations are concentrated between pairs of actin rods (Fig. 4*c*), allowing them to contribute to the effective binding, but in the swollen bundles with mutant lysozyme of charge +5e, the cations are localized completely around the actin rods (Fig. 4*d*), preventing them from exerting any binding effect. Whereas the present model can provide a qualitative picture, future improvements to these simulations could be made with computational models that include additional degrees of freedom to obtain a more accurate description of the swelling behavior in the presence of significant concentrations of salt.

These findings suggest a promising route toward destabilization of the actin–lysozyme complexes. Thus, we reduce the overall charge of lysozyme through site-directed mutagenesis and examine how this affects the electrostatic complexes. The monodispersity of these tailored macroions in charge as well as in size makes them particularly suited for comparison to model systems and greatly enhances the predictive capabilities of the simulations.

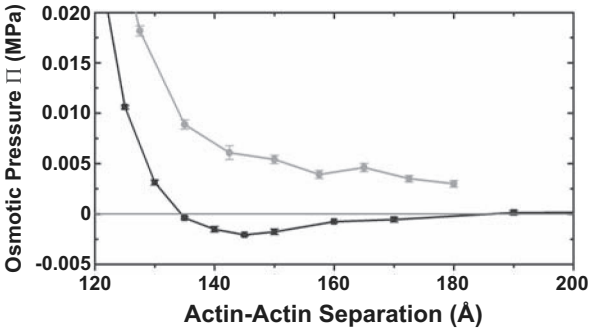

Fig. 3. Osmotic pressure of a hexagonally coordinated bundle of mutant (+5e) lysozyme–actin filaments in 0 mM salt (black line) and 5 mM salt (gray line) solutions, as determined from MD simulations. Negative pressure implies a contracting bundle, whereas $\Pi = 0$ MPa corresponds to a stable bundle. The zero crossing at a separation near 135 Å can be contrasted with the 100-Å separation for the WT lysozyme–actin complex at 0 mM salt as reported previously (9, 10). For the mutant lysozyme–actin, the addition of only 5 mM salt destabilizes the bundle (gray line).

SAXS Reveals That the Low-Stability Phase of Lysozyme–Actin Complexes Is Destabilized at a Wide Range of Salt Conditions. Fig. 2*a* shows 2D SAXS data from partially aligned isoelectric actin–lysozyme complexes made with the K16E/R119E double mutant (+5e), along with the diffracted intensity integrated along wedges in the q_z (Fig. 2*b*, black line) and q_r (Fig. 2*b*, gray line) directions, probed by using a 300×300 μm^2 synchrotron x-ray beam. Along the q_r direction, a strong diffraction feature is observed at $q \approx 0.065$ Å^{-1}, corresponding to an expanded inter-actin spacing of ≈111 Å. If we assume that the lysozyme remains at the threefold sites, this change would imply a ≈27% increase in the lateral lysozyme size, which is unlikely given the two amino acid mutations. However, the expanded lattice spacing is consistent with the swelling observed by the MD simulations (Fig. 2*d*), with lysozyme at the twofold bridging sites (depicted schematically in Fig. 2*c*). Along the q_z direction, a peak at $q \approx 0.126$ Å^{-1} is observed, reflecting a periodic arrangement of lysozyme along the F-actin axis that is comparable to that observed for WT lysozyme (which shows a peak at $q_z \approx 0.128$ Å^{-1}). Similar results are observed for two other +5e double mutants (K16E/K135E and K16E/R154E), which suggest that this structural change is attributable to nonspecific electrostatic effects. Interestingly, an even more swollen version of the twofold bridging phase with a further expanded lattice is observed for the K16E/K135E/K147E triple mutant with +3e charge at zero added salt (Fig. 2*e*). The intensity along the q_r direction shows a peak at $q \approx 0.063$ Å^{-1} (inter-actin spacing of ≈114 Å). The increased actin spacing compared with the +5e double mutants may indicate that lysozyme is bridging F-actin with the long axis of the lysozyme oriented at an angle to that of F-actin in the composite bundles. This phase, however, is unstable even for low concentrations of added salt: Fig. 2*e* shows that the complex dissociates at 25 mM monovalent salt.

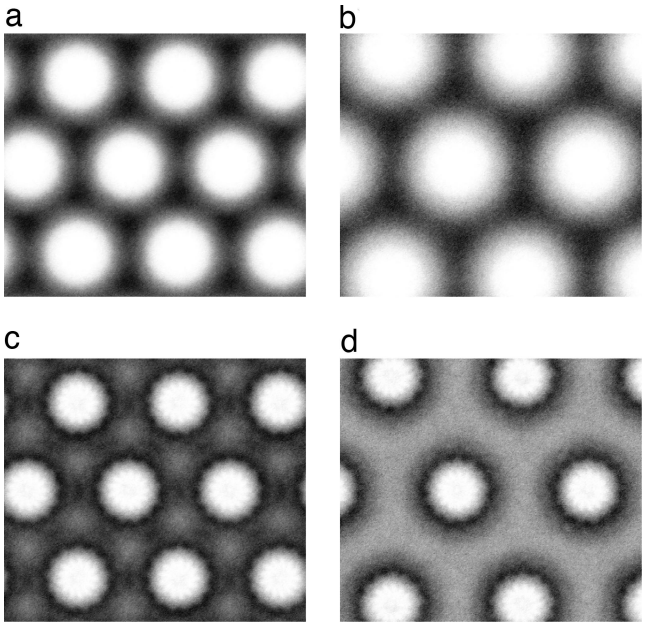

Fig. 4. Ionic density distributions (projected along the long axis of F-actin) within actin–lysozyme aggregates. (*a* and *b*) The anionic distribution for a stable actin bundle with WT lysozyme in the presence of 10 mM monovalent salt (*a*) and for an actin bundle containing mutant lysozyme in the presence of 5 mM monovalent salt (*b*). (*c* and *d*) The corresponding cation distributions. Although the anion distributions are homogeneous in both aggregates, the cation distributions show strong modulation and are different for both cases. In the WT lysozyme–actin complex, the cations are located predominantly between pairs of actin filaments (*c*), but for the mutant lysozyme actin bundle they are localized around individual filaments (*d*).

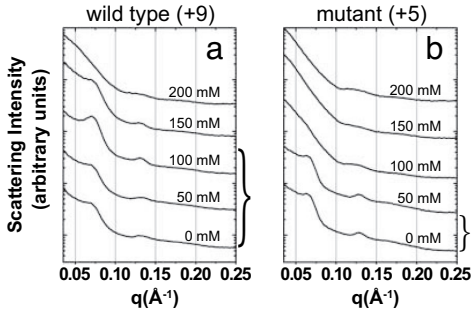

Fig. 5. Series of diffraction data showing evolution of bundle structure as a function of NaCl concentration for WT (+9e) lysozyme–actin complexes (*a*) and double-mutant (+5e) lysozyme–actin complexes (*b*). For the WT lysozyme–actin complexes (*a*), the maximum bundling occurs near ≈125 mM NaCl, whereas the mutant lysozyme–actin bundling peak (*b*) shows a maximum at ≈50 mM NaCl.

As predicted by the simulations, the change from threefold to twofold coordination of lysozyme within the bundle leads to a drastic change in the stability of the actin–lysozyme complex. Fig. 5 shows the SAXS spectra for electrostatic complexes formed between F-actin and WT (Fig. 5*a*) and a double-mutant (Fig. 5*b*) lysozyme at increasing concentrations of monovalent salt. For WT lysozyme, the bundle formation (and lysozyme sequestration) is maximized between 100 mM and 150 mM monovalent salt. [Results for NaCl are shown, but the same results also are observed for KCl (9, 10).] On the other hand, for the double mutant (+5e; Fig. 5*b*), bundle formation is maximized between 0 mM and 50 mM monovalent salt. The range of salt concentrations for which bundles form is larger than predicted by the simulations, which is consistent with the tendency of the coarse-grained model, already observed in ref. 10, to underestimate the precise range of stability. More importantly, however, the predicted trend is qualitatively confirmed by the experiments, and the mutant lysozyme unbinds from the actin, and thus is no longer sequestered, at the range of salt concentrations expected in the CF airway (50–150 mM). This finding suggests a potential method to make "nonstick" antimicrobials that will remain active in the electrostatic environment of the CF airway.

Direct Measurement of Lysozyme Sequestration and Antimicrobial Activity. For actin–lysozyme complexes at salt concentrations that mimic the range of physiological conditions, we examine whether

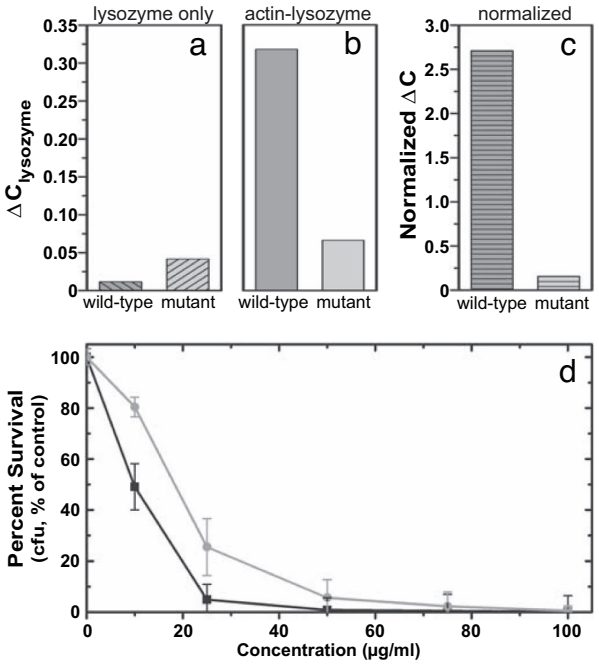

Fig. 6. Microequilibrium dialysis experiments indicate that charge-reduced lysozyme is drastically less susceptible to actin-induced sequestration than WT lysozyme is, which is measured by $\Delta C_{lysozyme} = (C_{experimental} - C_{theoretical})/C_{theoretical}$, where $C_{theoretical}$ is the expected concentration of a fully dialyzed solution (0.36 mg/ml) or ½ of the initial lysozyme concentration (0.72 mg/ml). $\Delta C_{lysozyme}$ is shown for dialysis of 0.72 mg/ml lysozyme solutions in the absence of actin (*a*) and in the presence of 1.4 mg/ml F-actin (*b*). (*c*) Results for the actin–lysozyme system normalized by those for the lysozyme-only system. This normalization corrects for potential differential adhesion of the different lysozyme to the dialysis membrane and shows a 17-fold decrease in sequestration for the mutant (light gray) relative to the WT (dark gray). (*d*) Results from antibacterial killing assays showing the percentage survival of PAO1 bacteria in the presence of increasing WT lysozyme (black line) and double-mutant lysozyme (gray line) concentrations. These results indicate that, despite structural changes, the double mutant retains most of the WT antibacterial activity.

the computational and SAXS findings are reflected by the degree of lysozyme sequestration. Microequilibrium dialysis experiments are used to measure the extent to which WT and mutant lysozyme remain sequestered by F-actin (Fig. 6 *a–c*). As a baseline measurement, WT and mutant lysozyme are dialyzed for 120 h against buffer in the absence of F-actin (Fig. 6*a*). In this case, the relative concentration difference $\Delta C_{lysozyme} = (C_{experimental} - C_{theoretical})/C_{theoretical}$ is very small, indicating that both WT and mutant lysozyme are nearly fully dialyzed. In contrast, if lysozyme is dialyzed from actin–lysozyme complexes (Fig. 6*b*), $\Delta C_{lysozyme}$ shows a large decrease in the amount of dialyzed WT lysozyme, reflecting the strong sequestration of WT lysozyme by the actin filaments. On the other hand, the much weaker binding of mutant lysozyme is confirmed by the weak increase of $\Delta C_{lysozyme}$. In Fig. 6*c*, we normalize the dialysis results obtained in the presence of actin (Fig. 6*b*) by those for lysozyme only (Fig. 6*a*), which shows that for WT lysozyme the degree of sequestration as measured by the deviation from a homogeneous distribution is ≈17 times larger than that for the mutant lysozyme.

The reduced adhesion of genetically engineered lysozyme to actin results in an increased availability of lysozyme. To assess whether this can translate into increased antimicrobial activity, it is necessary to evaluate whether the structural modifications of charge-reduced mutant lysozyme have not ablated its antibacterial activity. We perform bacterial killing assays on the PAO1 strain of *P. aeruginosa*, a Gram-negative bacterium commonly found in CF airway infections. Fig. 6*d* shows the averaged results from a series of 20 trials in which bacterial survival is monitored as a function of increasing protein concentration. The killing efficiency for the +5e mutant charge-reduced lysozyme (Fig. 6*d*, gray line) is comparable to, albeit slightly lower than, that of the WT +9e lysozyme (Fig. 6*d*, black line). Moreover, at a concentration of 100 μg/ml, the +5e mutant kills nearly all of the bacteria. These results suggest that it is indeed possible to optimize the charge distribution in antimicrobials to simultaneously minimize adventitious binding to inflammatory polymers and maintain antimicrobial activity.

Materials and Methods

The methodology of the MD and grand-canonical simulations has been provided in detail in ref. 10. The mutant lysozyme was modeled identically to the WT lysozyme (9, 10) but with a +2.5e charge on each of the two subunits.

Bacteriophage T4 pseudo WT lysozyme carried a charge of +9e at neutral pH and had dimensions of 30 × 30 × 50 Å^3 and a molecular weight of 18,700 (22). Expression and purification procedures of the WT lysozyme and its charge-reduced mutants were performed as reported (22). The charge mutants included three double mutants (K16E/R119E, K16E/R135E, and K16E/R154E) and one triple mutant (K16E/K135E/K147E); K, E, and R denote the amino acids lysine, glutamic acid, and arginine, respectively, and, for example, R154E denotes a mutation where the arginine at position 154 was replaced with glutamic acid.

Monomeric actin (G-actin) (M_r 43,000) was prepared from a lyophilized powder of rabbit skeletal muscle (Cytoskeleton, Denver, CO) as previously reported (9, 10).

The F-actin–lysozyme isoelectric point was at a molar ratio of 1.85:1 for F-actin:WT and 1:1 for F-actin:double mutant. Typical final concentrations were: F-actin, 5.6 mg/ml; WT lysozyme, 3.0 mg/ml; and double mutant, 5.4 mg/ml. These values are close to those found in the airway. A series of samples was prepared with the final monovalent salt concentration ranging from 0 mM to 200 mM. Lysozyme–actin complexes were sealed in 1.5-mm quartz capillaries (Hilgenberg, Malsfeld, Germany) and mixed thoroughly by centrifugation. The approximate sample volume in the capillary was 30 μl.

SAXS measurements were performed with beamline 4–2 at the Stanford Synchrotron Radiation Laboratory (Palo Alto, CA) and beamline 12-ID-C at the Advanced Photon Source (Argonne National Laboratory, Argonne, IL). For the Stanford Synchrotron Radiation Laboratory experiments (incident x-ray wavelength λ = 1.3806 Å), the scattered radiation was collected by using a MAR Research (Evanston, IL) charge-coupled device (CCD) camera (pixel size = 79 × 79 μm^2). For the Advanced Photon Source experiments (incident x-ray wavelength λ = 1.033 Å), the scattered x-rays were collected by using a MAR Research 2D mosaic CCD detector (pixel size = 79 × 79 μm^2). The 2D SAXS data from both setups were checked for mutual consistency. Additional details have been reported elsewhere (9, 10).

In collaboration with Donald Davidson (Carle Clinic Association, Urbana, IL) and in accordance with institutional review board-approved protocols at both Carle Clinic and at the University of Illinois at Urbana–Champaign, we collected mucus from CF patients who had not been treated with DNase (Pulmozyme; Genentech, Inc., South San Francisco, CA) for study by synchrotron x-ray microdiffraction. Patients voluntarily expectorated ≈5–10 ml of sputum during respiratory therapy. After collection, the sputum samples were rapidly frozen and stored at −80°C until use. Frozen samples were ultramicrotomed and sealed between kapton polyamide film (Dupont, Wilmington, DE).

Microdiffraction experiments of CF sputum samples were performed at beamline 2-ID-D at the Advanced Photon Source by using a beam size of 0.5 × 0.5 μm^2 focused with a Fresnel zone plate in conjunction with an order-sorting aperture. The sample-to-

detector distance was ≈420 mm corresponding to $q \approx 0.3$ Å^{-1}. Grid scans were taken about a center point with a 100-μm step size in both the horizontal and vertical directions.

Equilibrium dialysis was performed in microdialyzers (Harvard Apparatus, Boston, MA) containing two 100-μl chambers separated by a 50,000-Da cutoff cellulose acetate membrane. The "sample" chamber contained protein solutions in 100 mM NaCl/2 mM Tris buffer; the "assay" chamber contained only the 100 mM NaCl/2 mM Tris buffer. The protein solutions were either actin–lysozyme complexes (1.4 mg/ml actin/0.72 mg/ml lysozyme) or lysozyme-only controls (0.72 mg/ml). Protein solutions were allowed to dialyze against the NaCl/Tris buffer for 6 days to ensure complete dialysis. Protein concentrations were measured by using UV-visible spectroscopy at 280 nm.

The bactericidal activities of WT and mutant lysozyme were tested by using a microdilution killing assay on *P. aeruginosa* strain PAO1. Bacteria were grown in cation-adjusted Mueller–Hinton broth from an overnight culture (1:100 dilution) to mid-log phase at 37°C, harvested by centrifuging at 9,250 × *g* for 10 min, and resuspended in PBS (10 mM Na_2HPO_4/100 mM NaCl, pH 7.4). Bacteria were diluted so that 10^5 cfu were present in a final volume of 150 μl of the assay buffer, PBS. Bacteria were incubated with lysozyme in sterile 96-well flat-bottom polypropylene dishes while shaking for 3 h at 37°C. After the incubation period, bacteria were serially diluted, dropped on Mueller–Hinton agar plates, and incubated 18 h at 37°C, and colony-forming units were determined by using plate-counting methods.

We thank Dr. Brian W. Matthews (University of Oregon, Eugene, OR) for providing the T4 lysozyme plasmids and Dr. John K. Sheehan and Dr. C. William Davis (University of North Carolina, Chapel Hill, NC) for providing human mucins. We also gratefully acknowledge Dr. Michael J. Welsh and Dr. Pradeep K. Singh for insightful discussions and Dr. Zhonghou Cai, Dr. Barry Lai, Dr. Donald Davidson, Janice Douglas, Blaise Bowles, Leslie Gay, Scott C. Slimmer, John C. Butler, Thomas E. Angelini, Jae-Wook Lee, and Evelyn Huang for technical assistance. This material is based on work supported by the National Institutes of Health under Grant 1R21DK6843-01 (to G.C.L.W.), the Cystic Fibrosis Foundation (G.C.L.W.), and the National Science Foundation under Grants DMR-0346914 (to E.L.), DMR-0409769 (to G.C.L.W.), and CTS-0120978 (to E.L. and G.C.L.W.) via the WaterCAMPWS Science and Technology Center. Portions of this research were carried out at the Stanford Synchrotron Radiation Laboratory and at the Advanced Photon Source. The Stanford Synchrotron Radiation Laboratory Structural Molecular Biology Program is supported by the U.S. Department of Energy, Office of Biological and Environmental Research, and by the National Institutes of Health, National Center for Research Resources, Biomedical Technology Program. Use of the Advanced Photon Source is supported by the U.S. Department of Energy, Office of Basic Energy Sciences, under Contract DE-AC02-06CH11357.

1. Wong GCL (2006) *Curr Opin Col Int Sci* 11:310–315.
2. Grosberg AY, Nguyen TT, Shklovskii BI (2002) *Rev Mod Phys* 74:329–345.
3. Levin Y (2002) *Rep Prog Phys* 65:1577–1632.
4. Bloomfield VA (1996) *Curr Opin Struct Biol* 6:334–341.
5. Gelbart WM, Bruinsma RF, Pincus PA, Parsegian VA (2000) *Phys Today* 53:38–44.
6. Olvera de la Cruz M, Belloni L, Delsanti M, Dalbiez JP, Spalla O, Drifford M (1995) *J Chem Phys* 103:5781–5791.
7. Angelini TE, Liang H, Wriggers W, Wong GCL (2003) *Proc Natl Acad Sci USA* 100:8634–8637.
8. Angelini TE, Golestanian R, Coridan RH, Butler JC, Beraud A, Krisch M, Sinn H, Schweizer KS, Wong GCL (2006) *Proc Natl Acad Sci USA* 103:7962–7967.
9. Sanders LK, Guáqueta C, Angelini TE, Lee J-W, Slimmer SC, Luijten E, Wong GCL (2005) *Phys Rev Lett* 95:108302.
10. Guáqueta C, Sanders LK, Wong GCL, Luijten E (2006) *Biophys J* 90:4630–4638.
11. Welsh MJ, Smith AE (1995) *Sci Am* 273(6):52–59.
12. Vasconcellos CA, Allen PG, Wohl ME, Drazen JM, Janmey PA, Stossel TP (1994) *Science* 263:969–971.
13. Brandt T, Breitenstein S, von der Hardt H, Tummler B (1995) *Thorax* 50:880–882.
14. Shak S, Capon DJ, Hellmiss R, Marsters SA, Baker CL (1990) *Proc Natl Acad Sci USA* 87:9188–9192.
15. Sheils CA, Käs J, Travassos W, Allen PG, Janmey PA, Wohl ME, Stossel TP (1996) *Am J Pathol* 148:919–927.
16. Felgentreff K, Beisswenger C, Griese M, Gulder T, Bringmann G, Bals R (2006) *Peptides* 27:3100–3106.
17. Tang JX, Wen Q, Bennett A, Kim B, Sheils CA, Bucki R, Janmey PA (2005) *Am J Physiol* 289:L599–L605.
18. Travis SM, Singh PK, Welsh MJ (2001) *Curr Opin Immunol* 13:89–95.
19. Brogan TD, Ryley HC, Neale L, Yassa J (1975) *Thorax* 30:72–79.
20. Weiner DJ, Bucki R, Janmey PA (2003) *Am J Respir Cell Mol Biol* 28:738–745.
21. Bucki R, Byfield FJ, Janmey PA (2007) *Eur Respir J* 29:624–632.
22. Sun DP, Söderlind E, Baase WA, Wozniak JA, Sauer U, Matthews BW (1991) *J Mol Biol* 221:873–887.
23. Matthews BW, Remington SJ (1974) *Proc Natl Acad Sci USA* 71:4178–4182.
24. Broughton-Head VJ, Smith JR, Shur J, Shute JK (September 9, 2006) *Pulm Pharmacol Ther*, 10.1016/j.pupt.2006.08.008.
25. Angelini TE, Liang H, Wriggers W, Wong GCL (2005) *Eur Phys J B* 16:389–400.
26. Purdy KR, Bartles JR, Wong GCL (2007) *Phys Rev Lett* 98:058105.